OPEN ACCESS
IOP Publishing
Measurement Science and Technology
Meas. Sci. Technol. **36** (2025) 046134 (14pp)
https://doi.org/10.1088/1361-6501/adc75c

# Calibration strategy for a nondestructive wood characterization tool using optimized time-of-flight determination and material propagation analysis

**Irene Gil-Martín**[1,2], **Elisabet Suarez**[2,*] **and Andrés Roldán**[1]

[1] Department of Electronics and Computer Technology, University of Granada, Granada 18071, Spain
[2] Building Engineering School, University of Granada, Campus Fuentenueva s/n, 18071 Granada, Spain

E-mail: elisabetsv@ugr.es

Received 27 January 2025, revised 10 March 2025
Accepted for publication 31 March 2025
Published 10 April 2025

**Abstract**

Instrument calibration is essential to ensure measurement accuracy and reliability, particularly in wood characterization using non-destructive acoustic techniques. This study aims to develop and validate an improved calibration strategy for wood characterization tools. It focuses on integrating advanced algorithms into resource-constrained microcontroller systems. An optimized time-of-flight (ToF) detection algorithm based on the Akaike Information criterion (AIC) was implemented. The algorithm incorporates adaptive intelligent windows to autonomously identify the onset of acoustic waves, eliminating user intervention and enhancing repeatability. A suitable calibration material compatible with commercial piezoelectric sensors was identified and adapted for testing. Experimental investigations were carried out on cylindrical rods of various materials and lengths to measure acoustic wave propagation velocity, comparing results from two commercial systems and a laboratory-developed prototype. ToF measurements obtained with the prototype showed a high level of agreement with theoretical propagation times, outperforming commercial systems in accuracy and computational efficiency. These findings support the use of an aluminum bar as the reference calibration material, alongside the intelligent AIC algorithm, to ensure consistent and reliable measurements. The proposed calibration strategy offers a robust and repeatable solution for wood characterization applications. By optimizing computational efficiency and accuracy, this approach enables the integration of advanced acoustic measurement techniques into cost-effective, microcontroller-based systems, paving the way for broader adoption in industrial and research settings.

Keywords: non-destructive evaluation, acoustic emission, time of flight, computational cost, piezoelectric sensor, FTC algorithm, Akaike information criterion AIC

* Author to whom any correspondence should be addressed.

Original content from this work may be used under the terms of the Creative Commons Attribution 4.0 licence. Any further distribution of this work must maintain attribution to the author(s) and the title of the work, journal citation and DOI.


© 2025 The Author(s). Published by IOP Publishing Ltd

## 1. Introduction

The increasing demand for high-quality wood materials in various industries calls for innovative methods that guarantee the reliability and consistency of wood properties across the entire production chain, from silviculture to final product manufacturing [1–3]. Measuring the quality of trees throughout their growth and plantation years is crucial, as it enables the optimization of silvicultural practices and the production of higher-quality wood [4]. Early and continuous characterization of trees during their development can lead to better management strategies, ensuring that the wood harvested at maturity meets the desired standards [5]. This approach not only improves the overall health and productivity of forests, but also contributes to the creation of wood materials with enhanced mechanical and physical attributes. Non-destructive testing (NDT) technologies, particularly those based on acoustic emission (AE) techniques, have emerged as effective tools for this purpose [6, 7]. These methods provide valuable insights into the material's properties without causing any damage, making them an essential component of modern wood quality control [5].

A central aspect of AE NDT is the measurement of the time of flight (ToF) of an acoustic wave as it propagates through a material [8]. ToF represents the elapsed time it takes for an acoustic wave to travel from its source to a designated detector, typically a piezoelectric sensor. This measurement is a key indicator of the material's internal structure and mechanical properties [9]. The propagation velocity of the acoustic wave, which is inversely related to the ToF, can reveal important information about material homogeneity and the presence of internal defects. A reduction in ToF may indicate an elongated wave path, often caused by material heterogeneities or defects [10].

For the effective application of acoustic NDT, particularly for the assessment of mechanical properties such as stiffness and strength, precise detection of the wave's onset time is crucial [10–12]. Accurate identification of when the wave begins to propagate enables reliable measurements, facilitating a precise and non-destructive evaluation of various materials' properties. This becomes especially challenging when working with intelligent, autonomous algorithms that must process this information on a portable, embedded system with limited computational resources.

One of the biggest challenges in AE measurements is signal processing, which remains a key issue in the damage assessment and materials characterization. Much work is required to further improve the analysis of parameters and waveforms in AE signal processing, especially with regard to the normalisation of extracted features [13]. Some studies have focused on developing algorithms for accurate ToF determination, often relying on computationally expensive methods [14–16] or requiring user intervention for parameters selection [11, 17–22], reducing repeatability and automation.

This study addresses these limitations by introducing a novel calibration strategy that integrates an optimized ToF detection algorithm based on the Akaike Information Criterion (AIC) with adaptive intelligent windows. This autonomous approach identifies acoustic wave onset, enhancing repeatability and eliminating user intervention. However, this study goes beyond merely evaluating the effectiveness of such algorithms; it also aims to identify a feasible solution that can be embedded in low-computational-cost systems. This includes the development of algorithms capable of accurately interpreting ToF data under different conditions, ensuring robust and reliable assessments even in resource-constrained embedded environments.

This work addresses the development of a robust calibration strategy for an emerging prototype designed to perform non-destructive characterization of wood. Accurate calibration ensures the reliability and repeatability of results, essential for adoption in both industrial and research settings. The objectives of this study are summarized as follows:

(1) Optimization of intelligent autonomous algorithms for the accurate and reliable acquisition of the acoustic wave's onset time captured by piezoelectric sensors. A comparison of the computation time and the reliability of the results was carried out to embed the algorithm in a limited computational result system.
(2) Experimental determination of the acoustic wave's propagation velocity in cylindrical calibration rods of commercial materials by non-destructive acoustic techniques.
(3) A benchmark of various commercial devices and the emerging tool for obtaining the ToF in different materials and its accuracy.

By addressing the growing demand for precise and efficient quality control in wood production, this study advances acoustic measurement science and offers a scalable solution for structural health monitoring, material characterization, and industrial applications.

## 2. Method and materials

### *2.1. Structural quality characterization of a material*

The modulus of elasticity (MoE) is a mechanical property that indicates a material's stiffness. In the context of civil engineering, this property is indispensable for the design of structures that need to support large loads without undergoing deformations. Choosing the most economical and sustainable materials when designing a structure requires studying their MoE since it indicates the material's ability to resist deformations under loads. The higher the stiffness, the higher the MoE value [23].

This characteristic of materials relates stress-strain properties when they have a linear relationship [24]. The relationship is expressed in two ways, depending on the nature of the test performed on the material:

- **Modulus of static elasticity** ($MoE_{sta}$): subjected to deformation tests in a tensile strength testing machine [25].

$$MoE_{sta} = \frac{\sigma}{\varepsilon} \tag{1}$$

where σ is the normal stress and ε is the strain.

- **Modulus of dynamic elasticity** ($MoE_{dyn}$): obtained by dynamic methods involving the propagation of elastic waves [25].

$$MoE_{dyn} = {v_{prop}}^2 \cdot \rho \tag{2}$$

where $v_{prop}$ is the propagation velocity and $\rho$ is the density of the sample.

Because the procedure for obtaining the same property depends on the test carried out, the resulting numerical value will be similar but not the same. Numerous works correlate dynamic and static MoE values and show that it is possible to predict the MoE value from non-destructive tests [26–28]. Previous studies show that the dynamic MoE tends to be slightly higher than the static MoE [12, 29].

### 2.2. Description of the acoustic techniques

NDT based on acoustic techniques aims to determine the properties of a material by measuring its acoustic parameters such as the wave's propagation velocity or the wave's resonance frequency propagated inside the material. In this context, the propagation velocity is an intrinsic property of the material that is directly related to its $MoE_{dyn}$ [28]. The wave propagation velocity in the material is determined non-destructively as follows:

$$v_{prop} = \frac{\text{distance}}{\text{ToF}} \tag{3}$$

considering the distance between the sensors and the ToF as the time required for the wave to travel that distance.

A shorter propagation time implies a higher propagation velocity, which is associated with fewer general defects (such as knots, cracks, splits, or fibre deviations) in the material. Therefore, to achieve high-quality structural wood products, the propagation velocity should be maximized, which in turn will result in a higher MoE value.

In the wood value chain, NDT to assess wood quality can be performed at different stages: on the standing tree, on the log, or on the board. Figure 1 illustrates the measurement of ToF on a standing tree [26], which is the main objective of the equipment under development. The test consists of placing two piezoelectric sensors on the material: one near the emitting source (S1) and the other one at a set distance (S2).

Under controlled laboratory conditions and with the aim of establishing a measurement protocol to calibrate the device, tests were performed with different non-destructive equipment.

Figures 2(a) and (b) show the laboratory tests on a bar [23] using the AE equipment and the novel NDT tool, respectively.

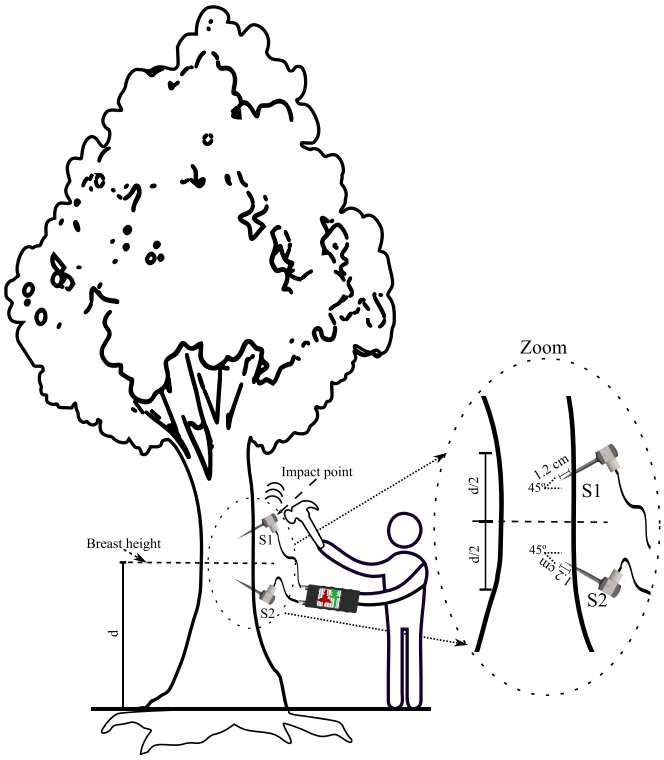


**Figure 1.** Scenario for wood quality measurement in standing trees using non-destructive acoustic techniques.

A wave is artificially generated at or near S1. Both sensors capture the wave, although a delayed and attenuated version of the wave detected at S1 is recorded at S2 figure 2(c). This delay corresponds to the ToF value, calculated from the onset time of each wave as.

$$\text{ToF} = t_{\text{init},S2} - t_{\text{init},S1} \tag{4}$$

where $t_{\text{init},S2}$ is the wave's onset time captured by sensor S2 and $t_{\text{init},S1}$ is the wave's onset time captured by S1.

### 2.3. ToF algorithms for determining an acoustic wave onset time

As previously indicated, it is necessary to find an algorithm that can automatically and accurately estimate the waves' onset time, $t_1$ and $t_2$ (figure 2(c)). Detecting the onset time is not trivial, since an inaccurate algorithm can lead to an erroneous calculation of the acoustic wave propagation velocity, and consequently of the MoE. Therefore, in this paper, two algorithms are proposed to estimate the onset time of the signal:

- **First Threshold Cross (FTC) algorithm:** This algorithm is widely used due to its simplicity. The ToF can be estimated from the time when the raw signal crosses a previously defined amplitude threshold [17]. The selection of an appropriate threshold for each kind of signal requires a thorough analysis of the signals according to the environment and the

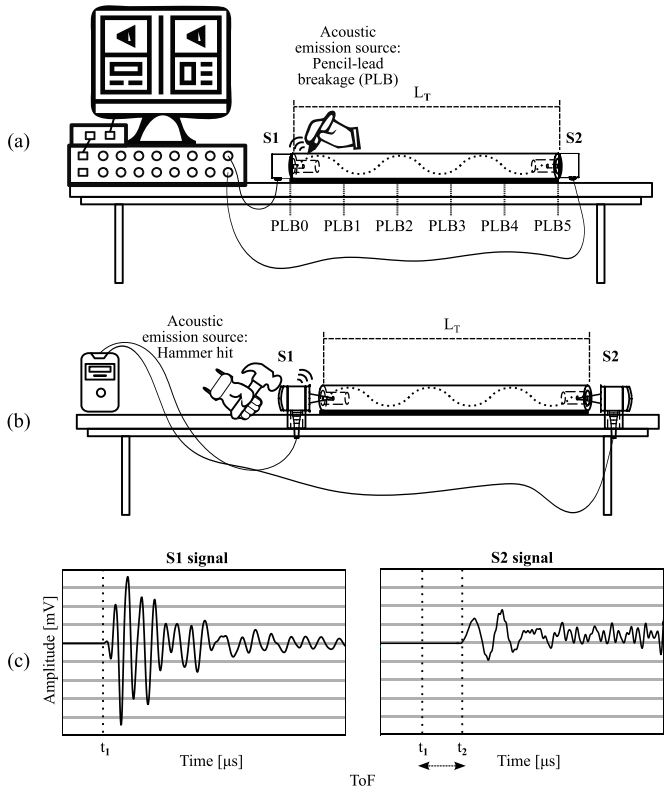


**Figure 2.** (a) Experimental set-up of the ToF measurement test on a bar using the acoustic emission equipment and a pencil-lead breakage (PLB) as source; (b) Experimental set-up of the ToF measurement test using the novel NDT characterization tool and a hammer hit as source; (c) Examples of waves captured by each sensor with indication of the arrival time of each wave and the ToF between them.

material [18, 19]. This method is theoretically simple and requires low computational time, which makes it an efficient and practical option for computer implementation.

- **AIC algorithm**: The AIC algorithm can effectively separate different events in a transient signal or determine the signal arrival time [30–32]. This statistical method divides the signal at a point of entropy change: high entropy is expected in the noisy signal region, to the left of the signal start, while low entropy is expected on the right, after the transient signal start [18].

The function that allows estimating the entropy difference in a signal is defined as:

$$\mathrm{AIC}(k) = k \cdot \log\left(\sigma^2(x[1:k])\right) + (N-k-1) \cdot \log\left(\sigma^2(x[K+1:N])\right) \quad (5)$$

where $N$ is the total sample count of the signal, and k represents the order of each sample, ranging from 1 to $N$. The signal onset time is related to maximum entropy, and therefore the AIC function will reach its minimum value. The AIC algorithm requires the selection of a signal window. In the literature, many studies have estimated the window sample length based on visual observation [20–22]. However, changes in the sampling frequency or selecting a window that is too small to capture the event can lead to errors in determining the wave onset time. In order to eliminate the inconvenience of visual window selection, this paper proposes a novel improvement by means of automatic window selection based on the maximum amplitude of the signal, which is close to the start of the signal. Two versions of the algorithm are proposed: a fixed window (AIC F.W.) visually selected as described in the literature [20]; and a newly proposed intelligent and autonomous variable window (AIC V.W.) valid for any kind and for any sampling rate.

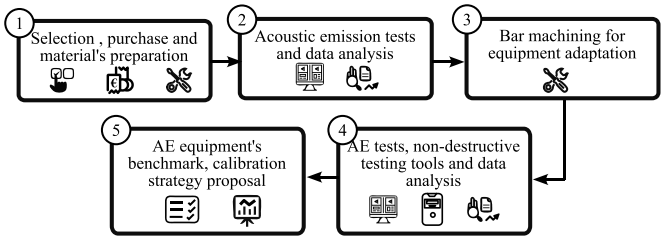


**Figure 3.** Phases followed in the study of the calibration strategy for a non-destructive testing tool to characterize wood.

Numerous papers have already analyzed acoustic signals using AIC algorithms [18, 33, 34]. Specifically, a comparison between FTC and AIC algorithms focused on wood [19]. No references have been found that evaluate the vulnerability of the AIC algorithm to sampling frequency variations. The existence of different levels of background noise has been studied, although the proposed method involves a high computational cost [33, 35]. While the AIC algorithm is intended to detect various types of changes, there is limited analysis on how to address multiple changes within the specific portion of the signal where the algorithm is applied.

In this paper, the comparison in terms of measurement accuracy will be analyzed, as well as aspects related to the computational cost of both algorithms in order to evaluate the minimum characteristics of the systems used to implement them. Previous research has investigated the computational time of AIC [31], but without considering the feasibility of its integration into a system with limited resources.

### *2.4. Experimental procedure*

The calibration strategy developed entailed five phases, as illustrated in figure 3, explained in detail in section 2.5. First, various materials were selected as potential calibration bars, and these materials were prepared in the form of bars of different lengths (section 2.5). Next, several acoustic tests were conducted, and data analysis was performed to assess the reliability and repeatability of the experimental measurements (section 2.6). Given the need for a wooden block to insert the piezoelectric sensors, the bars were modified through machining. Non-destructive tests were subsequently conducted with the new configuration, and the resulting data were analyzed. Finally, a comparison of the results obtained with different

**Table 1.** Materials used for the calibration bars, including properties, diameters, and prices.

| Material | Description | | | | | | |
|---|---|---|---|---|---|---|---|
| | Isotropy | Homogeneity | Density (g cm$^{-3}$) | MoE$_{sta}$ (GPa) | Diameter (mm) | Price (€/m) | Propagation velocity (m s$^{-1}$) |
| Stainless steel AISI-304 | ✓ | ✓ | 7.93[b] | 193[b] | 25 | 34.83[c] | 4933 |
| Aluminum 7075 T6 | ✓ | ✓ | 2.80[a] | 72[a] | 25 | 18.85[c] | 5000 |
| Perlitic cast iron (GG) | ✓ | ✓ | 7.20[a] | [100–120][a] | 25 | 11.89[c] | [3727–4085] |
| Brass (CuZn39Pb2) | ✓ | ✓ | 8.45[b] | 102[b] | 25 | 48.51[c] | 3475 |
| Plastic Delrin POM C | ✘ | ✓ | [1.41–1.43][a] | 3[a] | 25 | 6.57[c] | 1459 |
| Beechwood | ✘ | ✘ | [0.71–0.73][b] | $14.8 \cdot 10^{-3}$[b] | 25 | 2.59[c] | [4566–4503] |

[a] Information given by the manufacturer.
[b] Information obtained from bibliographic sources.
[c] Prices excluding taxes and transportation charges, referred to June 2022.

equipment was carried out, leading to the establishment of the calibration strategy.

### 2.5. Material description

To select the most suitable calibration bar in terms of material and length, cylindrical rods made from various commercial materials were chosen. NDT was conducted on these rods to assess the acoustic wave propagation velocities. Table 1 lists the six materials analyzed, along with their respective properties, covering a broad range of densities, elastic moduli, costs, and acoustic propagation velocities. Beechwood was used to adapt the bars to the positioning requirements of the sensors for wooden applications, not as a material for the calibration bar. For each of the 5 materials selected for the calibration bars, six different bar lengths were prepared, ranging from 150 mm to 1479 mm, as shown in figure 4. Figure 5 provides a real image of the bars of varying lengths and materials. The initial tests in phase 2 were performed with the bars of constant cross-section (figure 4(b)). However, as the commercial piezoelectric sensors used for wood applications specifically the SD-02 sensors from Fakopp (figure 6) need to be inserted into wood, the bars were adapted to incorporate a piece of wood. To this end a machining procedure was proposed as phase 3, shown in figure 4(c). This procedure involves drilling cylindrical holes at both ends of the bars, into which beechwood cylinders were inserted, ensuring proper placement of the sensors, and enabling them to capture the propagating acoustic waves within the material. To enhance wood-to-metal adhesion and ensure the bar behaves as a single element under vibrations, a thin layer of silicone grease was applied as a coupling agent between the metal and the wood.

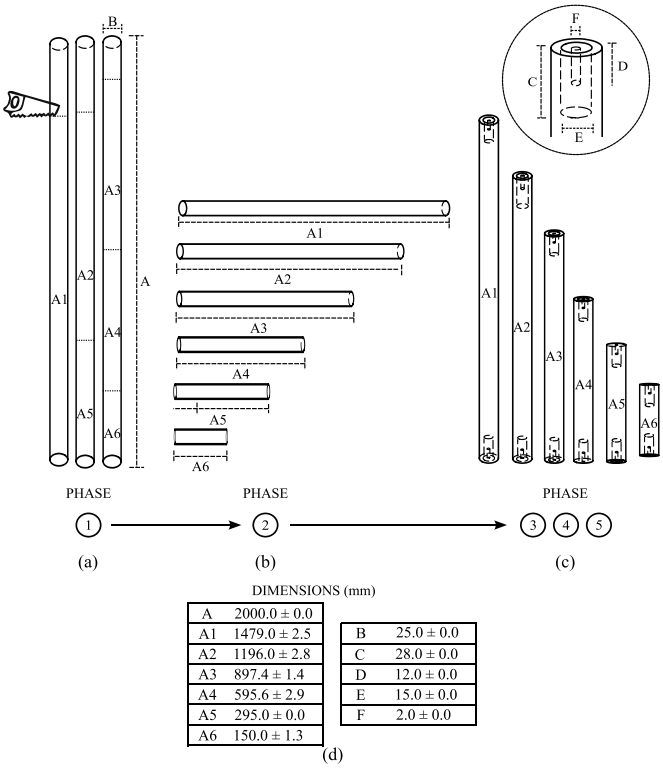


**Figure 4.** Scheme of the bar preparation process following phases described in figure 3: (a) bars prepared for cutting; (b) bars with different lengths; (c) machined bar with a detail image of the machining section; (d) table with the dimensions indicated in the diagram by letters, all in mm.

### 2.6. NDT equipment for wood quality characterization

Three measurement devices were selected for this research: a commercial laboratory AE system for obtaining highly accurate data (AE equipment, described in section 2.6.1); a commercial NDT tool that measures acoustic wave propagation times (MST tool, described in section 2.6.2); and a prototype developed in our laboratory for conducting non-destructive acoustic tests, designed to be a user-friendly field device that delivers comprehensive technical results (TIK TREE, described in section 2.6.3).

*2.6.1. Vallen systeme AE equipment.* The AE equipment used to characterize the materials is the Vallen Systeme AMSY-6. VS-150M piezoelectric sensors with a 150 kHz frequency resonance [37] were placed on the surface to acquire the wave (figure 7). A layer of silicone grease is placed between the material and the sensor to ensure proper wave propagation. For a correct sensor-equipment interface, the AEP4 amplifiers were used with a gain of 34 dB [38].

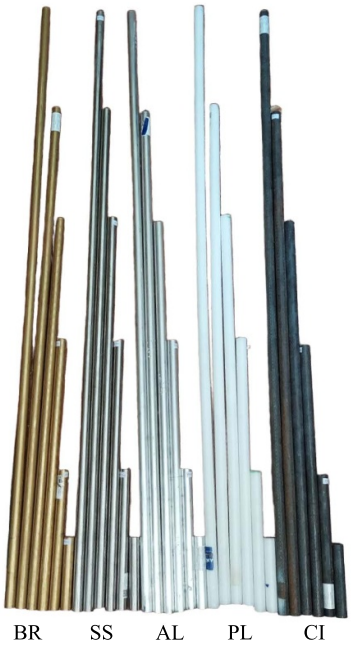


**Figure 5.** Real image of the bars with different lengths. Materials: BR refers to brass, SS to stainless steel, AL to aluminum, PL to plastic, and CI to pearlitic cast iron (GG).

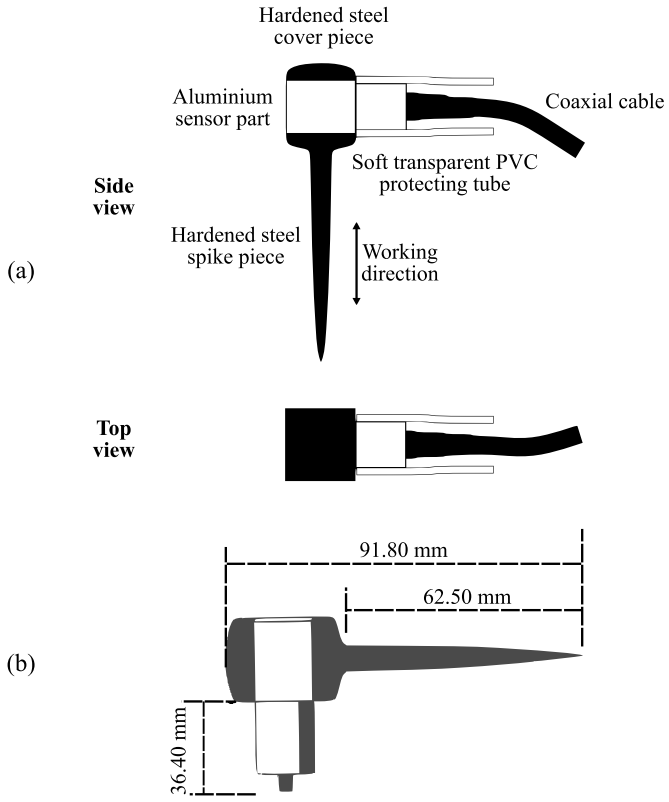


**Figure 6.** SD-02 piezoelectric sensor from Fakopp. (a) Side view and top view [36]; (b) Dimensions for the side view, all in mm.

Figure 8 shows the AE tests' experimental set-up for phases 2 and 4. Once the wave was recorded, the signals were processed using the different algorithms to obtain the ToF in each case.

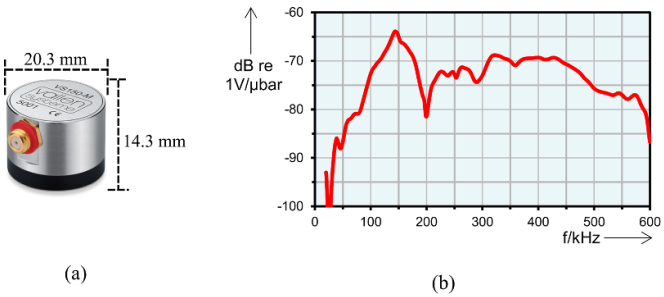


**Figure 7.** VS-150M sensor from Vallen Systeme. (a) Real view of the sensor; (b) Frequency spectrum of the sensor.

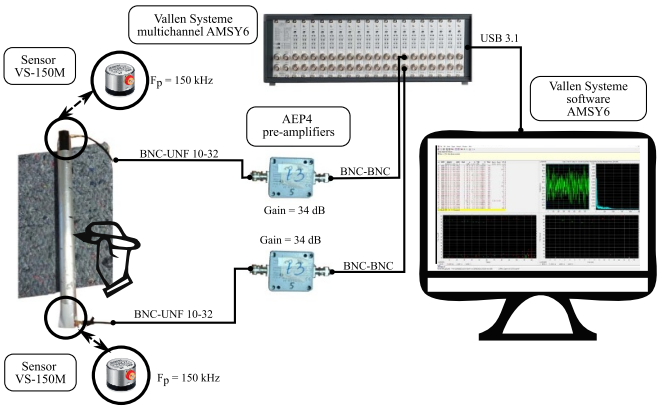


**Figure 8.** Experimental set-up for AE tests.

As the AE source,pencil-lead breakage (PLB) was used, it being a long-established standard as the reproducible artificial source for different applications. Often this type of source is also referred to as the Hsu-Nielsen source, based on the original works of Hsu and Nielsen [39]. These types of signals obtained using PLBs are highly reproducible if the manipulation of the lead holder is accurately repeated [40].

After the instrumentation was installed, a PLB test was performed as a calibration procedure to verify proper functionality. EA tests were conducted on all the bars at six distinct, equidistant positions between the sensors, as shown in figure 2(a). At each position, five breakages were carried out, resulting in a total of 30 data points for each bar.

*2.6.2. Fakopp microsecond timer (MST) NDT tool.* MST is a NDT tool for evaluation of trees from Fakopp company. It was designed to help determine the structural soundness of trees by measuring the ToF of an acoustic wave. The measured time is indicative of solid wood, or a problem area caused by decay, fungus, or other structural damage [36]. This tool only provides the propagation time between the two sensors, not giving any information about the recorded waves or the time determination procedure.

The sensors used in this test were the model SD-02 from Fakopp, shown in figure 6, with a resonant frequency of 23 kHz. The experimental set-up used in Phase 4 is shown in figure 9.

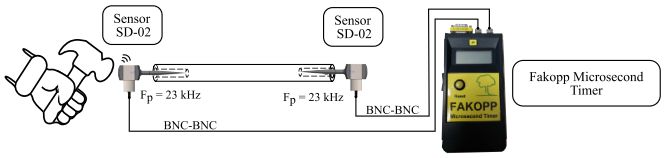


**Figure 9.** Experimental setup for tests using MST tool.

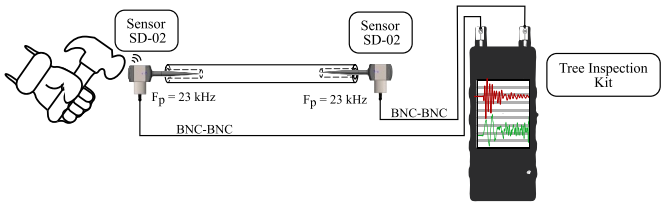


**Figure 10.** Experimental setup for the laboratory-developed non-destructive AE testing tool.

The SD-02 sensors must be driven into the material under study at a depth of 12 mm parallel to the bar. A hit of a hammer of 100 g on one of the sensors was used as an acoustic source. In this case, 5 repetitions were carried out on each sensor. Therefore, a total of 10 measurements per bar were registered.

The calibration method proposed with this equipment is based on the use of an optional calibration bar provided by the manufacturer. The manual of the equipment indicates the time (with known error) to be recorded during the calibration test. When the calibration time indicated by the manufacturer is obtained, the equipment is ready to give reliable measurements. If the measured ToF does not match the calibration time, the user must add manual post-processing in the office, where the results must be corrected by adding or subtracting the value obtained in the calibration test [33]. This procedure hinders measurements in that the real values are not obtained in the field and can lead to errors.

*2.6.3. TIK TREE, an NDT tool prototype.* TIK Tree is an emerging tool for non-destructive wood characterization. This portable, innovative, and low-cost device was used with the commercial SD-02 sensors (figure 6) by Fakopp. The experimental setup of the Phase 4 tests using the prototype equipment is shown in figure 10.

The measurement procedure is the same as in the previous section. That is, each sensor is hit 5 times on each of the bars; hence there will be 10 measurements per bar.

Finally, it should be noted that the calibration of this equipment will depend on the study carried out in this research. The idea is to include an easy-to-handle bar (laboratory-measured with the equipment) allowing the user to perform a calibration experiment. The calibration mode is selected from the general menu before proceeding to perform the calibration test. The tool measures the ToF of the propagated wave and compares it with the factory setting. The difference will be adjusted automatically within the equipment, assuring accurate and reliable results.

## 3. Results and discussion

### *3.1. Optimization and reliability validation of ToF determination algorithms*

In this research, three options of algorithms are proposed for determining the onset time of an acoustic wave the FTC algorithm [17–19] and two versions of the AIC algorithm [30–32] along with two alternatives: fixed window (AIC F.W.) or variable window (AIC V.W.). The aim of the first analysis is to determine the most accurate algorithm and appraise whether the computational cost is reasonable to embed it into a system with limited computational resources. This section addresses their advantages and disadvantages, including statistical analysis of the computation time.

Figure 11 offers an example of the transient signals recorded during the AE test carried out on the 148 cm length aluminum bar, including the threshold, the AIC values and the ToF using all three algorithms. The upper signal comes from the S1 sensor, closest to the source. The signal below was recorded by S2, being farthest from the source. The dashed curve lines represent the AIC values. As seen, the onset time is set at the point where the minimum AIC value is reached. The vertical lines indicate the onset times of the signal applying the three proposed algorithm versions.

Observing signal S1, the FTC algorithm and the optimized AIC V.W. algorithm estimated the onset of the wave with good accuracy. However, the AIC F.W. algorithm (not optimised) did not properly detect the onset in the S1 registered wave. Observing the AIC F.W. values, a minimum found at 2.9 µs would be related to the onset of the signal, but the global minimum is obtained at 175.5 µs, associated with a change in amplitude of the wave (attenuation of the signal). Automatically, the algorithm selects as ToF the global minimum of AIC, so the automatic detection using a fixed window is erroneous. This fact supports the statement that the visual selection of the windows to apply the AIC algorithm can induce errors in certain cases. The fact of considering the window size ($N$) in the AIC calculation has already been recognized in previous studies [11, 41], where these values have been shown to significantly influence the AIC results, which underlines the importance of taking them into account when applying the algorithm [27].

It should be stressed that for the FTC algorithm, the signal was visually studied, and the threshold was chosen conscientiously. Despite this, in some cases (like the S2 sensor signal) the FTC algorithm had indicated a start prior to where the signal actually started. Setting the threshold in a generic way is very complicated, especially for signals propagated in non-homogeneous media.

Note that the difference between the AIC V.W. and the AIC F.W. algorithms is the number of events that lead to a change in signal entropy. As the theory of this criterion dictates, for good results, the part of the signal containing the event to be detected must be analyzed [10]. As an example, table 2 presents the mean values and standard deviation (STD) obtained for aluminum bars of different lengths, applying the three algorithms and comparing them with the theoretical value. It can be observed that the STD

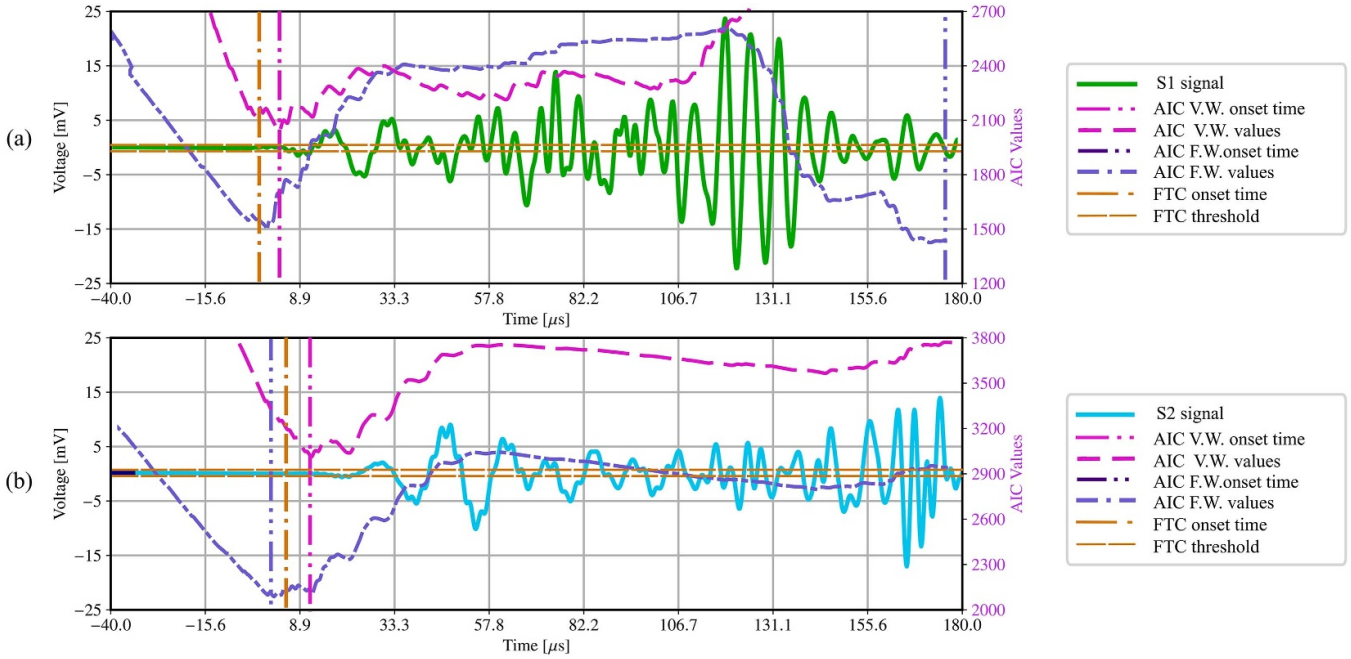


**Figure 11.** Examples of the transient signals recorded during the AE test carried out on the 148 cm length aluminum bar, the threshold, the AIC values, and the ToF using the three algorithms. (a) Signal coming from S1, the sensor closest to the source; (b) Signal coming from S2, farthest from the source.

**Table 2.** ToF measured on bar of aluminum of different lengths calculated applying the AIC F.W., AI C.V., and TOF, along with theoretical values.

| Length (cm) | Algorithm | AIC F.W. (μs) | AIC V.W. (μs) | FTC (μs) | Theoretical (μs) |
|---|---|---|---|---|---|
| 147.9 | Mean | 244.4 | 279.9 | 279.8 | 291.5 |
| | STD | 79.4 | 3.7 | 3.7 | — |
| 119.6 | Media | 238.3 | 238.5 | 238.5 | 235.1 |
| | STD | 38.2 | 4.0 | 4.0 | — |
| 89.7 | Media | 150.3 | 179.3 | 179.6 | 177.1 |
| | STD | 68.0 | 4.5 | 4.7 | — |
| 59.6 | Media | 66.3 | 118.4 | 118.3 | 117.7 |
| | STD | 74.8 | 7.8 | 7.8 | — |
| 29.5 | Media | 52.6 | 52.5 | 52.6 | 58.2 |
| | STD | 3.1 | 3.1 | 3.0 | — |
| 15.0 | Media | 24.4 | 24.5 | 24.5 | 29.2 |
| | STD | 1.1 | 0.9 | 0.9 | — |

values obtained with AIC F.W., where a fixed window is applied in all cases, are more than 20 times higher for the 147.9 cm bars and approximately 10 times higher for the 119.6 cm, 89.7 cm, and 59.6 cm bars, compared to the AIC V.W. and FTC algorithms. Therefore, in terms of measurement accuracy, the optimized AIC V.W. algorithm should be taken as the one that detects the wave onset with the highest accuracy.

In terms of computational time, figure 12 shows a graph of the computation time required by each algorithm, having run 500 iterations of each algorithm on the same signals. This procedure was repeated for four runs. Therefore, the computation time was estimated for a total of 2000 runs of each algorithm on the same signals.

The computer used for the measurements had a 13th generation Intel i7-1355U 1.70 GHz processor with an installed RAM of 32 GB (31.6 GB usable) and a 64-bit operating system with an x64-based processor. The operating system used was Windows 11 multitask system, resources far beyond what any microcontroller can offer.

The significant changes in time as measured from one iteration to another were a result of Windows background multitasking processes, which introduced uncontrolled and undesirable interruptions.

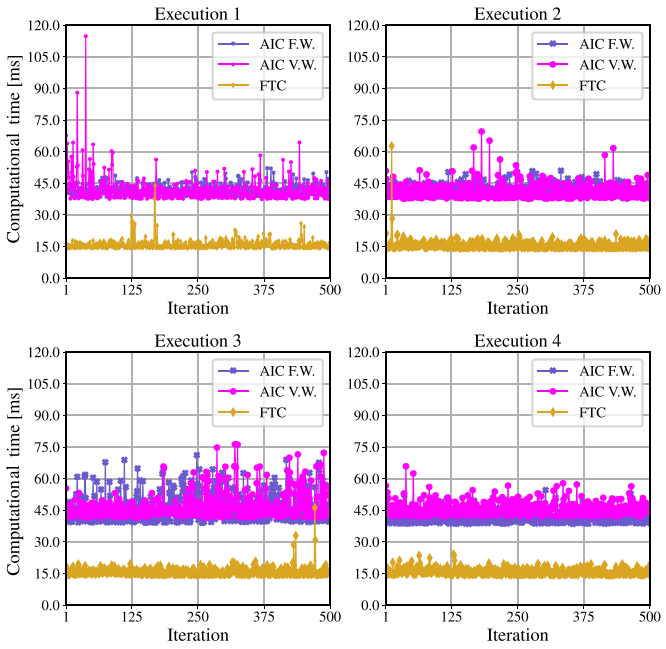


**Figure 12.** Computational time of the AIC F.W., AIC V.W. and FTC algorithms on four executions of 500 repetitions each, of the signals recorded on the AE test carried out with 29.5 cm length AISI-304 stainless steel bars.

From a temporal computational perspective, the FTC algorithm is the least time-consuming, processing 4096 samples in an average time of 14 ms. In contrast, both versions of the AIC algorithm take around 60 ms per run (AIC F.W. processes 2000 samples, while AIC V.W. less than 1000 samples). Although the AIC algorithm is four times slower than the FTC algorithm, it could be successfully used with a lower-resource system such as the TIK Tree tool.

Considering these results, in the following sections only the AIC V.W. and FTC algorithms are compared. The AIC F.W. algorithm was rejected due to its inefficiency and high margin of error.

### *3.2. Estimation of the propagation velocity of an acoustic wave in different materials*

AE tests were carried out to measure the propagation velocity inside cylindrical bars of different isotropic and homogeneous commercial materials, following the indications of section 2.6.1. Table 3 shows the ToF measured on the bars of different materials and lengths, applying the AIC V.W. and FTC algorithms.

It can be observed that the highest STD are obtained for the FTC algorithm, but they are not always larger for longer bars. For example, in the case of brass, higher STD values are found for 119.6 cm and 89.7 cm than for 149.7 cm, while for Plastic Delrin, the highest STD is observed at 119.6 cm. This indicates that high STD values are primarily associated with the algorithm used for ToF detection. These results highlight the limitations of the FTC algorithm, which is based on a fixed amplitude threshold and is particularly sensitive to wave dispersion, attenuation, and noise, as small changes in signal amplitude can lead to inconsistent results, in consonance with previous research [11, 29]. In contrast, the proposed autonomous approach, the AIC V.W. algorithm, is more robust against these effects, providing greater accuracy and repeatability across different sample lengths and materials.

Figure 13 displays, as an example, the ToF results obtained for the aluminum 7075 T6 bars of different lengths, including both the theoretical values and those obtained with the AIC V.W. and FTC algorithms. The propagation velocity was obtained as the inverse of the slope of the linear regression ($y = mx + n$) of the bar's length and the ToF measured in each, considering all 30 repetitions carried out.

$$\mathrm{ToF} = m \cdot L + n \tag{6}$$

where $m$ is the regression slope, $L$ is the length of the bar and $n$ is the error term.

The coefficient of determination ($R^2$) is also indicated. The $R^2$ value for the theoretical values is not presented, as it is always 1. In this case, it is evident that the dispersion between ToF values is very low, except for the longest bars. It may be because, as the bar length increases, factors such as attenuation, resonance frequencies, or propagation modes have a more significant effect.

Table 4 shows the theoretical and experimental velocity values obtained with the AIC V.W. and FTC algorithms for each material, including the $R^2$ value. As seen, the experimentally obtained velocities through NDT, in percentage variation, differ significantly from the theoretical values [42–46]. The variation remains below 5% in all metallic materials except for iron, which reaches 14%. This low dispersion in metals was expected, as they are homogeneous materials. However, the high dispersion in iron is due to the pearlite-ferrite ratio in its composition, which has a strong influence on the propagation velocity. If the theoretical velocity does not precisely match the composition of the material supplied, variations in

**Table 3.** ToF measured on bars of different materials and lengths, applying the AIC V.W. and FTC algorithms (mean ± STD), along with theoretical values.

| Materials | Stainless steel AISI-304 | | | Aluminium 7075 T6 | | | Perlitic cast iron (GG) | | | Brass (CuZn39Pb2) | | | Plastic Delrin POM C | | |
|---|---|---|---|---|---|---|---|---|---|---|---|---|---|---|---|
| Lengths (cm) | Theor. (μs) | AIC V.W. (μs) | FTC (μs) | Theor. (μs) | AIC V.W. (μs) | FTC (μs) | Theor. (μs) | AIC V.W. (μs) | FTC (μs) | Theor. (μs) | AIC V.W. (μs) | FTC (μs) | Theor. (μs) | AIC V.W. (μs) | FTC (μs) |
| 149.7 | 299.2 | 316.2 ± 4.9 | 307.6 ± 33.3 | 291.5 | 279.7 ± 3.7 | 279.8 ± 3.7 | 379.6 | 332.2 ± 5.0 | 328.2 ± 44.9 | 425.0 | 442.1 ± 13.4 | 419.7 ± 30.4 | 995.4 | 881.0 ± 34.4 | 879.5 ± 34.3 |
| 119.6 | 243.3 | 260.2 ± 5.5 | 252.9 ± 17.4 | 235.1 | 238.5 ± 4.0 | 238.5 ± 4.0 | 306.9 | 277.7 ± 7.3 | 272.4 ± 31.8 | 343.9 | 357.6 ± 11.1 | 343.6 ± 30.7 | 809.3 | 706.2 ± 36.1 | 704.3 ± 37.6 |
| 89.7 | 181.8 | 194.4 ± 7.1 | 182.0 ± 20.7 | 177.1 | 179.3 ± 4.5 | 179.6 ± 4.7 | 230.0 | 208.1 ± 7.5 | 198.4 ± 24.6 | 258.4 | 269.6 ± 14.4 | 258.6 ± 35.7 | 604.9 | 447.9 ± 17.8 | 447.6 ± 17.7 |
| 59.6 | 121.2 | 130.4 ± 5.4 | 130.0 ± 17.5 | 117.7 | 118.4 ± 7.8 | 118.3 ± 7.8 | 153.2 | 144.0 ± 33.2 | 148.5 ± 44.4 | 171.8 | 172.9 ± 11.7 | 157.7 ± 14.7 | 403.3 | 270.7 ± 6.1 | 270.7 ± 6.1 |
| 29.5 | 59.8 | 56.4 ± 2.2 | 56.4 ± 2.2 | 58.2 | 52.5 ± 3.1 | 52.6 ± 3.0 | 75.6 | 62.1 ± 2.6 | 62.1 ± 2.7 | 84.9 | 73.7 ± 3.0 | 73.6 ± 2.9 | 198.9 | 134.1 ± 3.2 | 134.1 ± 3.2 |
| 15.0 | 30.4 | 26.3 ± 1.8 | 26.3 ± 1.8 | 29.2 | 24.5 ± 0.9 | 24.5 ± 0.9 | 38.4 | 30.8 ± 4.4 | 30.9 ± 4.4 | 43.2 | 35.3 ± 2.6 | 35.4 ± 2.7 | 101.2 | 65.3 ± 3.2 | 65.2 ± 3.2 |

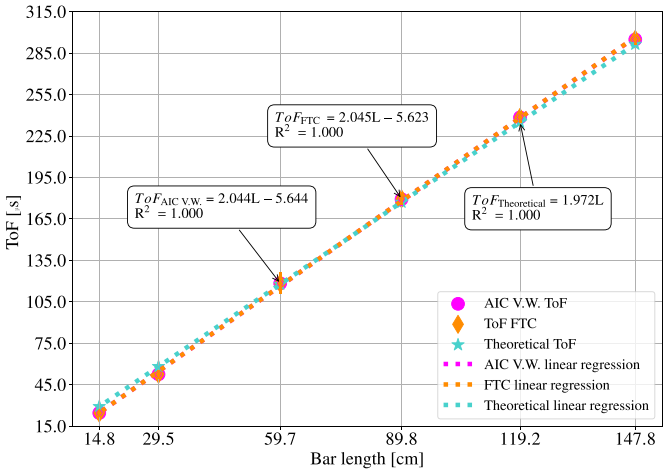


**Figure 13.** Bar length vs. ToF measured during the AE tests on the 7075 T6 aluminium bar, including the estimated theoretical values as well as the values calculated using the AIC V.W. and FTC algorithms.

**Table 4.** Propagation velocities for all materials: theoretical (obtained from the static MoE) and experimental values, obtained as the inverse of the regression slope of the regression line estimated for each material.

| Algorithm | Theoretical | AIC Variable Window | | | FTC | | |
|---|---|---|---|---|---|---|---|
| Materials | Mean propagation velocity (m $s^{-1}$) | Mean propagation velocity (m $s^{-1}$) | $R^2$ | Variation from Theoretical velocity (%) | Mean propagation velocity (m $s^{-1}$) | $R^2$ | Variation from Theoretical velocity (%) |
| Stainless steel AISI-304 | 4933.4 | 4539.3 | 1.000 | 8.0 | 4712.5 | 0.999 | 4.5 |
| Aluminium 7075 T6 | 5075.9 | 5091.6 | 0.998 | 0.3 | 5091.6 | 0.998 | 0.3 |
| Pearlitic cast iron (GG) | 3904.7 | 4347.8 | 0.999 | 11.3 | 4450.4 | 0.998 | 14.0 |
| Brass (CuZn39Pb2) | 3474.6 | 3228.9 | 1.000 | 7.1 | 3397.4 | 1.000 | 2.2 |
| Plastic Delrin POM C | 1428.8 | 1607.7 | 0.994 | 12.5 | 1610.3 | 0.995 | 12.7 |

the measured velocity can occur, as demonstrated in [47]. On the other hand, the variation in plastic exceeding 12% is reasonable due to its non-homogeneous nature and the variability of its physical properties depending on the temperature process [46].

This finding is consistent with the expected difference [11, 12, 29] since, although the property is the same, the methods used to obtain it inherently produce variations in the resulting values. Moreover, the experimentally obtained velocities for steel, aluminum, and brass agree with those reported in other experimental studies [48, 49]. Reinforcing the reliability of the results for these homogeneous materials. In contrast, the larger deviation observed in iron and plastic further supports the influence of microstructural heterogeneity and material composition on wave propagation, highlighting the importance of precise characterization when comparing theoretical and experimental values.

It is also noteworthy that in the case of the AIC V.W. algorithm, the $R^2$ is closer to 1 than for the FTC, both being very good values of this parameter. Because the 29.5 cm bars are the most suitable for transport and handling, and present lower dispersion (STD) due to attenuation or mode interferences, from here on only the results on these bars will be analyzed.

**Figure 14.** Experimental scenario for measuring the influence of the waveguide of the SD-02 Fakopp sensors.

### *3.3. Experimental determination of the time propagation at the sensor waveguide*

Since the SD-02 sensor used for NDT in wood has a waveguide of considerable size (60 mm), it was investigated whether the propagation time at the tip of this sensor was despicable or not. The experimental scenario of this verification test is shown in figure 14. The time taken by the wave to travel through the

**Table 5.** ToF times measured on the bars of 29.5 cm length using the three different equipment types and two algorithms (AIC V.W. and FTC). (Mean values ± STD).

| Equipments | AE | | TIK | | MST |
|---|---|---|---|---|---|
| Materials | AIC V.W. (μs) | FTC (μs) | AIC V.W. (μs) | FTC (μs) | (μs) |
| Stainless steel AISI-304 | 84.7 ± 5.2 | 84.6 ± 5.1 | 80.5 ± 3.0 | 105.8 ± 13.1 | 73.3 ± 4.3 |
| Aluminium 7075 T6 | 70.7 ± 1.4 | 70.6 ± 1.3 | 71.9 ± 0.6 | 83.8 ± 1.7 | 71.4 ± 2.5 |
| Pearlitic cast iron (GG) | 92.5 ± 5.8 | 92.5 ± 5.8 | 92.8 ± 3.6 | 150.5 ± 10.7 | 84.2 ± 1.4 |
| Brass (CuZn39Pb2) | 113.9 ± 4.7 | 113.9 ± 4.8 | 103.8 ± 2.3 | 121.3 ± 6.5 | 99.3 ± 1.1 |
| Plastic DELRIM POM C | 253.1 ± 2.3 | 253.0 ± 2.3 | 194.8 ± 2.8 | 249.0 ± 3.9 | 180.6 ± 4.9 |

sensor tip was set to 14.1 ± 1.3 μs. This time value served to correct the measurements recorded using these sensors.

### *3.4. Benchmarking of the ToF on different materials using different NDT tools*

This section benchmarks the ToF values obtained from 29.5 cm long bars using different NDT tools. The tests were conducted with the AE equipment, following the configuration shown in figure 8, the commercial MST equipment (figure 9), and the laboratory-developed prototype TIK Tree (figure 10). A layer of acoustic couplant was applied between the bar and the wooden plugs (placed to allow the sensors to be driven in) in order to enhance wave propagation between the two materials.

The AE tests and those performed with the TIK tool enabled recording of the signals registered by the sensors. In both cases, the previously selected FTC and AIC V.W. algorithms were applied. The propagation time of the wave through the sensor tip was considered in the ToF calculation. While the MST equipment provides a ToF value, it does not allow for signal visualization.

Table 5 shows the ToF values measured on the 29.5 cm long bars, with the three devices, applying the calculation algorithms. Comparing the values obtained with AIC V.W. and FTC, for both in the AE and TIK tests, the AIC V.W. algorithm generally yields lower STD values, except in the cases of stainless steel and aluminum in the AE tests. This is consistent with findings in the literature, where it has been demonstrated that the STD of FTC is generally higher than that of AIC [11]. The TIK tool used with the AIC V.W. algorithm gives lower STD values when compared to the AE tests, except in the case of plastic. The threshold algorithm exhibits significantly higher STD values, reaching up to 10% of the mean value in the case of plastic. Thus, it can be said that AIC V.W. is more accurate, since the threshold algorithm depends on a threshold amplitude value chosen by the user. In signals recorded with a relatively low sampling frequency, very large errors can be obtained if an erroneous start sample is selected. Therefore, for a low sampling frequency, the threshold method should be discarded if the signal noise conditions are not well controlled. This finding aligns with observations in other studies, where it has been noted that the main advantage of AIC is its repeatability. As these algorithms provide consistent results for the same signal, they are particularly useful when interpreting complex signals, where multiple arrival points could be chosen manually, or in cases with very large datasets where manual interpretation becomes impractical [41].Table 6 presents the percentage differences in the ToF measured with the TIK and MST tools as opposed to the ToF measured with the AE system using the AIC V.W. algorithm. Overall, the ToFs measured using MST tool present a greater deviation than the ToF measured using TIK tool (except from aluminum), but with a difference of 1%. It can therefore be deduced that the new equipment proposal provides more accurate ToF estimates, closer to laboratory equipment, than the commercial tool MST.

**Table 6.** Variation (%) of the mean ToF measured with the TIK and MST tools compared to the ToF measured with the AE system using the AIC V.W. algorithm.

| | Variation from AE (%) | |
|---|---|---|
| Materials | TIK | MST |
| Stainless steel AISI-304 | 5 | 13 |
| Aluminum 7075 T6 | 2 | 1 |
| Pearlitic cast iron (GG) | 0 | 9 |
| Brass (CuZn39Pb2) | 9 | 13 |
| Plastic DELRIM POM C | 23 | 29 |

**Table 7.** Comparison of the dimensions, mass and price of the selected materials.

| Materials | L (cm) | D (mm) | m (kg) | Cost (€) |
|---|---|---|---|---|
| Stainless steel AISI-304 | 29.5 | 25 | 1.46 | 10.3 |
| Aluminum 7075 T6 | 29.5 | 25 | 0.52 | 5.56 |
| Pearlitic cast iron (GG) | 29.5 | 25 | 1.33 | 3.51 |
| Brass (CuZn39Pb2) | 29.5 | 25 | 1.56 | 14.3 |
| Plastic DELRIM POM C | 29.5 | 25 | 0.26 | 1.94 |

Finally, table 7 presents a comparison of the dimensions, mass, and cost of the studied materials to select the calibration bar of the TIK Tree tool. This table aims to support the material selection process, not only considering the repeatability and reproducibility of the measurements, but also identifying the most portable, manageable, and cost-effective material for production. It is evident that plastic is the cheapest and most manageable material. Yet according to the results in

table 4, which demonstrate that plastic did not provide repeatable measurements, it is deemed unsuitable for our purpose. Therefore, the next most lightweight and affordable material is aluminum, making it the most appropriate choice. The ToF measured by all equipment is very similar, so that it can be assured that ToF measurements carried out on cylindrical aluminum bars are repeatable and reproducible.

## 4. Conclusion

In this study, a calibration strategy was developed for a non-destructive wood characterization prototype tool based on acoustic measurements. To obtain a calibration bar suitable for the correct placement of the sensors, the influence of the bar machining process was investigated, including wooden plugs to facilitate this purpose. Three algorithms were evaluated to determine the arrival time of acoustic signals, highlighting an innovative approach based on the well-known AIC algorithm, enhanced by incorporating adaptive intelligent windows (AIC V.W.). The results demonstrated that the AIC V.W. algorithm provided more repeatable and reliable results and was suitable for integration into microcontrollers with limited resources. Several experimental tests were carried out to determine the acoustic wave propagation velocity in bars of different materials, comparing these values with theoretical velocities. In view of the analysis and discussion of the results, the proposed calibration strategy involves the use of an aluminum bar 29.5 cm in length and 25 mm in diameter, machined to include wooden plugs for the attachment of piezoelectric sensors.

## Data availability statement

The data that support the findings of this study are openly available at the following URL/DOI: https://granasat.space/2025/01/calibration-strategy-for-a-non-destructive-wood-characterization-tool-using-optimized-time-of-flight-determination-and-material-propagation-analysis/.

## Acknowledgment

The authors would like to thank the Structural Timber Research Unit of Andalusia (UIMA) and the Electronics Aerospace Group (GranaSAT) for their collaboration and for providing free access to their laboratory measurement equipment's.

## Fundings statement

This work has been carried out within the framework of the LIFE Wood for Future project 'Recovery of poplar groves in the Vega de Granada for the improvement of biodiversity and long-term carbon sequestration in structural bioproducts', financed by the LIFE Programme of the European Union [LIFE 20 CCM/ES/001656].

## Conflict of interest

We declare that we have no financial and personal relationships with other people or organizations that can inappropriately influence our work.

## ORCID iDs

Irene Gil-Martín https://orcid.org/0009-0007-7060-0502
Elisabet Suarez https://orcid.org/0000-0003-1725-7219
Andrés Roldán https://orcid.org/0000-0001-6807-7053

## References

[1] Makkonen M 2018 Stakeholder perspectives on the business potential of digitalization in the wood products industry *BioProducts Bus.* **5** 1–15
[2] Borz S A, Oghnoum M, Marcu M V, Lorincz A and Proto A R 2021 Performance of small-scale sawmilling operations: a case study on time consumption, productivity and main ergonomics for a manually driven bandsaw *Forests* **12** 810
[3] Navarro-Cerrillo R M, Cachinero-Vivar A M, Pérez-Priego Ó, Aspizua Cantón R, Begueria S and Julio Camarero J 2023 Developing alternatives to adaptive silviculture: thinning and tree growth resistance to drought in a Pinus species on an elevated gradient in Southern Spain *For. Ecol. Manage.* **537** 120936
[4] Gonçalves J L D M, Stape J L, Laclau J-P, Smethurst P and Gava J L 2004 Silvicultural effects on the productivity and wood quality of eucalypt plantations *For. Ecol. Manage.* **193** 45–61
[5] Balasso M, Hunt M, Jacobs A and O'Reilly-Wapstra J 2021 Development of non-destructive-testing based selection and grading strategies for plantation eucalyptus nitens sawn boards *Forests* **12** 343
[6] Brashaw B, Bucur V, Gonçalves R, Lu J, Meder R, Pellerin R, Potter S, Ross R, Wang X and Yin Y 2009 Nondestructive testing and evaluation of wood: a worldwide research update *For. Prod. J.* **59** 7–14
[7] Llana D F, Short I and Harte A M 2020 Use of non-destructive test methods on Irish hardwood standing trees and small-diameter round timber for prediction of mechanical properties *Ann. For. Sci.* **77** 62
[8] Papandrea S F, Cataldo M F, Bernardi B, Zimbalatti G and Proto A R 2022 The predictive accuracy of modulus of elasticity (MOE) in the wood of standing trees and logs *Forests* **13** 1273
[9] Essien C, Via B K, Cheng Q, Gallagher T, McDonald T and Eckhardt L 2018 Determining the predictive accuracy of whole tree modulus of elasticity (MOE) of 14-year-old loblolly pine using density and dynamic MOEs estimated by three different acoustic tools *Eur. J. Wood Wood Prod.* **76** 1535–46
[10] Arciniegas A, Prieto F, Brancheriau L and Lasaygues P 2014 Literature review of acoustic and ultrasonic tomography in standing trees *Trees* **28** 1559–67
[11] Zhu J, Li W, Mu K, Zhang X and Zhao X 2025 An automatic arrival time picking algorithm of ultrasonic waves for concrete crack depth detection *Eng. Struct.* **328** 119729
[12] Darmono, Ma'arif F, Widodo S and Nugroho M S 2019 Determination of modulus of dynamic elasticity of wood using ultrasonic pulse velocity testing *IOP Conf. Ser.: Earth Environ. Sci.* **366** 012015

[13] Laflamme S *et al* 2023 Roadmap on measurement technologies for next generation structural health monitoring systems *Meas. Sci. Technol.* **34** 093001
[14] Elfering M, Annas S, Jantzen H-A and Janoske U 2022 Method for time-of-flight estimation of low frequency acoustic signals in reverberant and noisy environment with sparse impulse response *Meas. Sci. Technol.* **33** 045101
[15] Luo J, Bespal'Ko A A, Lu D and Li B 2024 Method for the P-wave arrival pickup of rock fracture acoustic emission signals under strong noise *Meas. Sci. Technol.* **35** 086102
[16] Zonzini F, Bogomolov D, Dhamija T, Testoni N, De Marchi L and Marzani A 2022 Deep learning approaches for robust time of arrival estimation in acoustic emission monitoring *Sensors* **22** 1091
[17] Rescalvo F J, Ripoll M A, Suarez E and Gallego A 2019 Effect of location, clone, and measurement season on the propagation velocity of poplar trees using the Akaike information criterion for arrival time determination *Materials* **12** 356
[18] van Blokland J, Adamopoulos S, Olsson A, Oscarsson J and Källander B 2018 Evaluation of non-destructive test methods to predict bending properties of thermally modified timber *2018 World Conf. on Timber Engineering (WCTE)* (*Seoul, Republic of Korea*, *20–23 August 2018*)
[19] Yenn Chong S, Lee J-R and Chan Yik P 2013 Statistical threshold determination method through noise map generation for two dimensional amplitude and time-of-flight mapping of guided waves *J. Sound Vib.* **332** 1252–64
[20] Mborah C and Ge M 2018 Enhancing manual P-phase arrival detection and automatic onset time picking in noisy microseismic data in underground mines *Int. J. Min. Sci. Technol.* **28** 691–9
[21] Carpinteri A, Xu J, Lacidogna G and Manuello A 2012 Reliable onset time determination and source location of acoustic emissions in concrete structures *Cem. Concr. Compos.* **34** 529–37
[22] Khuc T, Nguyen P T, Nguyen A and Catbas F N 2020 A nonparametric method for identifying structural damage in bridges based on the best-fit auto-regressive models *Int. J. Struct. Stab. Dyn.* **20** 2042012
[23] Suárez Vargas E 2017 *Vibro-acoustic Methods Applied to Damage Assessment of Materials Used in Construction and Civil Engineering* (University of Granada)
[24] Hibbeler R C 2011 *Mechanics of Materials* 8th edn (Pearson) (https://doi.org/10.1016/j.mechmat.2010.12.004)
[25] Beer F, Johnston E, DeWolf J and Mazurek D 2014 *Mechanics of Materials* 5th edn (McGraw-Hill) p 82
[26] Meyers M A and Chawla K K 2009 *Mechanical Behavior of Materials* 2nd edn (Cambridge University Press) p 111
[27] Chauhan S and Sethy A 2016 Differences in dynamic modulus of elasticity determined by three vibration methods and their relationship with static modulus of elasticity *Maderas Cienc. Tecnol.* **18** 373–82
[28] Thomaz W D A, Miyaji D Y and Possan E 2021 Comparative study of dynamic and static Young's modulus of concrete containing basaltic aggregates *Case Stud. Constr. Mater.* **15** e00645
[29] Kánnár A and Csiha C 2021 Comparative analysis of static and dynamic moe of pannónia poplar timber from different plantations *Wood Res.* **66** 195–202
[30] Yan X and Xu X 2021 Method for accurately measuring of acoustic time difference based on optimal threshold *Measurement* **171** 108769
[31] Kolassa S 2011 Combining exponential smoothing forecasts using Akaike weights *Int. J. Forecast.* **27** 238–51
[32] Li X, Shang X, Morales-Esteban A and Wang Z 2017 Identifying P-phase arrival of weak events: the Akaike information criterion picking application based on the empirical mode decomposition *Comput. Geosci.* **100** 57–66
[33] Kim Y M, Han G, Kim H, Oh T-M, Kim J S and Kwon T H 2020 An integrated approach to real-time acoustic emission damage source localization in piled raft foundations *Appl. Sci.* **10** 8727
[34] Cheng A, Xu E, Yao P, Zhou Y, Huang S and Ye Z 2024 An automatic arrival time picking algorithm of P-wave based on adaptive characteristic function *Comput. Geosci.* **185** 105544
[35] Li H, Yang Z and Yan W 2022 An improved AIC onset-time picking method based on regression convolutional neural network *Mech. Syst. Signal Process.* **171** 108867
[36] Fakopp 2024 Microsecond timer manual (available at: https://files.fakopp.com/mstimer/)
[37] Vallen Systeme 2022 AE–sensor data sheet (available at: www.vallen.de/)
[38] Vallen Systeme 2022 AMSY-6 system specification (available at: www.vallen.de/)
[39] Hsu N N and Breckenridge F 1981 Characterization of acoustic emission sensors *Mater. Eval.* **39** 60–68
[40] Sause M G R 2011 Investigation of pencil-lead breaks as acoustic emission sources *J. Acoust. Emiss.* **29** 184–96
[41] Flood-Page G, Boutonnier L and Pereira J-M 2024 Application of the Akaike Information Criterion to the interpretation of bender element tests *Soil Dyn. Earthq. Eng.* **177** 108373
[42] Datasheet Stainless steel AISI-304 2022 Randrade (available at: www.randrade.com/)
[43] Datasheet Aluminium 7075 T6 2022 Randrade (available at: www.randrade.com/)
[44] Datasheet Pearlitic cast iron (GG) 2022 Randrade (available at: www.randrade.com/)
[45] Datasheet Brass (CuZn39Pb2) 2022 Randrade(available at: www.randrade.com/)
[46] Datasheet Plastic DELRIM POM C 2022 Randrade (available at: www.randrade.com/)
[47] Orłowicz W, Tupaj M and Mróz M 2010 Quality control by means of ultrasonic in the production of ductile iron *ISIJ Int.* **50** 906–12
[48] Nie W, Jones K C, Petro S, Kassaee A, Sehgal C M and Avery S 2018 Proton range verification in homogeneous materials through acoustic measurements *Phys. Med. Biol.* **63** 025036
[49] Deng L, Yuan H, Chen J, Meng X, Zhang M, Su G, Zhou Y, Zhou Y and Chen Y 2024 Multiple methods for acoustic emission source location in metal waveguides *Measurement* **229** 114444